analytical chemistry

Article

pubs.acs.org/ac

Sensitive Nanochannel Biosensor for T4 Polynucleotide Kinase Activity and Inhibition Detection

Lei Lin, Yang Liu, Jing Yan, Xingsheng Wang, and Jinghong Li*

Department of Chemistry, Beijing Key Laboratory for Analytical Methods and Instrumentation, Tsinghua University, Beijing 100084, China

Supporting Information

ABSTRACT: 5′-Polynucleotide kinase is a crucial class of enzyme that catalyzes the phosphorylation of nucleic acids with 5′-hydroxyl termini. This process regulates many important cellular events, especially DNA repair during strand damage and interruption. The activity and inhibition of nucleotide kinase have proven to be an evident effect on cellular nucleic acid regulation and metabolism. Here, we describe a novel nanochannel biosensor for monitoring the activity and inhibition of T4 polynucleotide kinase (PNK), a famous member of the 5′-kinase family playing a major role in the cellular responses to DNA damage. On the basis of the functionalized nanochannel system and coupled λ exonuclease cleavage reaction, the nanochannel-sensing platform exhibits high sensitivity and convenience toward kinase analysis. Biotin-labeled dsDNA effectively blocks the streptavidin-modified nanochannel through forming a closely packed arrangement of DNA structure inside the channel. When dsDNA is phosphorylated by PNK and then immediately cleaved by λ exonuclease, the pore-blocking effect almost disappears. This PNK-induced microstructural distinctness can be directly and accurately monitored by the nanochannel system, which benefits from its high sensitivity to the change of the effective pore size. Furthermore, modification convenience and mechanical robustness also ensure the stability of the test platform. This as-proposed strategy exhibits excellent analytical performance in both PNK activity analysis and inhibition evaluation. The simple and sensitive nanochannel biosensor shows great potential in developing on-chip, high-throughput assays for fundamental biochemical process research, molecular-target therapies, and clinic diagnostics.

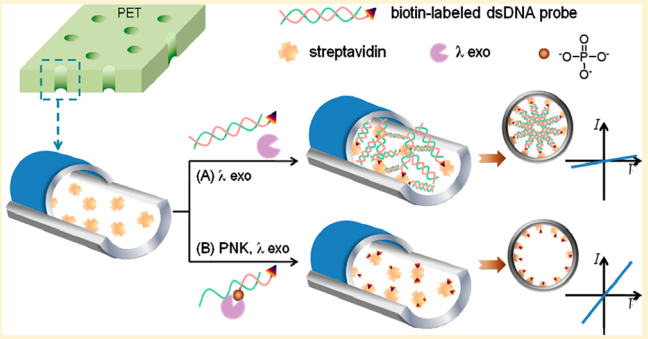

The 5′-polynucleotide kinase is a crucial class of enzyme that catalyzes the phosphorylation of nucleic acids with 5′-hydroxyl termini. This process regulates many important cellular events, especially DNA repair during strand damage and interruption,[1−4] which result from various exogenous and endogenous agents including chemical substances,[5] ionizing radiation,[6] as well as nucleases.[7] Normal function of 5′-polynucleotide kinase is indispensable to the 5′-phosphate terminal dependent DNA healing and the maintenance of gene integrity. Blockage of DNA phosphorylation may lead to serious consequences, even some lethal diseases. T4 polynucleotide kinase (PNK), first discovered in 1965,[8] is a famous member of the 5′-kinase family. It catalyzes the transfer of the γ-phosphate group of nucleoside triphosphate (ATP) to the 5′-hydroxyl end of oligonucleotides or nucleic acids. PNK has been extensive used in analysis of DNA adducts[9] and in repair of nucleic acid lesions.[10] What's more, PNK plays a major role in cellular nucleic acid metabolism, particularly in the cellular responses to DNA damage. Aberrant PNK activity and DNA phosphorylation states relate to many human disorders as Bloom's syndrome, Werner syndrome, and Rothmund-Thomson syndrome.[11] Accordingly, information about the activity profile of PNK and its potential inhibitors is not only useful for investigating the fundamental biochemical process during nucleic acid metabolism but also valuable for the development of effective therapeutic protocols and kinase-targeted drug discovery.

Until now, various approaches for the determination of DNA phosphorylation have been developed. Conventionally, the activity of PNK was detected by radical isotope ^{32}P-labeling, polyacrylamide gel electrophoresis (PAGE), and autoradiography.[3,4,8,12−16] Although these methods work well in both in vitro and in vivo analytical systems, unfortunately, complicated instruments, sophisticated operating procedures, and always in need of skillful technicians greatly limit their wide applications. Furthermore, these approaches also suffer from other disadvantages such as radioactive contamination, time-consuming, and costly. Recently, to eliminate the traditional problems, fluorescence assays have emerged as an increasingly popular tool for evaluating DNA phosphorylation. Song et al. described a novel fluorescence approach for real-time monitoring of the kinetics of PNK based on specially designed DNA-hairpin probes and coupled enzyme reaction.[17] Wu et al. successfully

Received: October 3, 2012
Accepted: November 29, 2012
Published: November 29, 2012

   dx.doi.org/10.1021/ac302875p | Anal. Chem. 2013, 85, 334−340

screened DNA phosphorylation process by using graphene oxide as a super quencher.[18] However, fluorescence signals are largely influenced by many environmental factors in the reaction system. Various undesirable substances would make the fluorescence signals unreliable. In addition, the increasing demands of practical applications require further development of a sensing platform with much better analytical performance. Therefore, more avenues still need to be explored to have a convenient, rapid, sensitive and accurate method to measure the activity of DNA phosphorylation kinase.

In recent years, artificial nanochannels fabricated in track-etched polymer membranes have received unrivalled research attention due to their unique properties, for instance, well-defined geometries and dimensions, ease of miniaturization, and compatibility with electronic measurement technique.[19−21] Furthermore, fabrication simplicity and modification convenience greatly enrich the nanochannel systems in the field of biomimetic materials.[22−24] Comparing with protein nanochannels, which still have to rely on the fragile lipid bilayer, solid-state nanochannel appears to be much more promising in practical applications because of its mechanical and chemical robustness. Artificial nanochannels modified with appropriate functional groups have emerged as an increasingly popular tool to develop innovative sensing platforms for analysis of proteins,[25] DNA,[26] ions,[27,28] and small molecules.[29,30] Unfortunately, despite its notable advantages, the nanochannel based platform has not yet been applied to detect the activity and inhibition of important kinases.

In this work, we designed a novel nanochannel biosensor for detecting PNK activity and inhibition on the basis of functionalized nanochannel systems combined with the λ exonuclease (λ exo, a highly processive 5′-3′ enzyme catalyzing the removal of 5′ mononucleotides from duplex DNA to generate single-stranded DNA (ssDNA) and mononucleotides) cleavage reaction. Taking advantage of the efficient affinity interaction, biotin-labeled double-stranded DNA (biotin-dsDNA) effectively blocked the streptavidin-modified nanochannel through forming a closely packed arrangement of dsDNA structure inside the channel. Nevertheless, when PNK and λ exo cleavage reaction were introduced, the blockage effect almost disappeared because of the prompt digestion of biotin-dsDNA by the coupled enzymes. Owing to its sensitive response to microstructural distinctness, the nanochannel sensing system not only provides an excellent PNK screening platform with wide linear range and low detection limit but also shows super ability for accurate investigation of kinase-targeted inhibitors. Moreover, modification convenience and mechanical robustness also ensure the stability of the test platform. The simple and sensitive nanochannel biosensor exhibits great potential in biological processes research and drug discovery.

EXPERIMENTAL SECTION

Reagents. T4 polynucleotide kinase (10 units/μL), λ exonuclease (5 units/μL) were bought from New England Biolabs (NEB, U.K.). *N*-Hydroxysuccinimide (NHS) and *N*-ethyl-*N*-(3-dimethylaminopropyl)carbodiimide (EDC) were purchased from Alfa Aesar. Tris(hydroxymethyl)aminomethane (Tris), adenosine triphosphate (ATP), adenosine diphosphate (ADP), dithiothreitol (DTT), 2-[*N*-morpholino]ethanesulfonic acid (MES), and streptavidin were obtained from Beijing DingGuo Biotech. Co., Ltd. Polyethylene terephthalate membranes (PET; Hostaphan RN 12, Hoechst, 12 μm thick, with ion track of 10^6/cm^2) were bought from GSI, Darmstadt. The DNA sequences were purchased from Shanghai Sangon Biological Engineering Technology & Services Co., Ltd. Other regents of analytical grade were obtained from Beijing Chemical Company (China). Sequences of oligonucleotide probes used in this work are listed as follows:

Probe 1 (P1-biotin): 5′-GCT ACT AGT AAT CTT GTT CAT AGT ATC ATT GTA CAT AGT GTC AGA GCC-biotin-3′

Probe 2 (P2): 5′-C3-GGC TCT GAC ACT ATG TAC AAT GAT ACT ATG AAC AAG ATT ACT AGT AGC-3′

Probe 3 (P3-FAM): 5′-AAC AAG ATT ACT AGT AGC-FAM-3′

Current Measurements. A nanoporous PET film was mounted between two chambers of the testing cell which are both filled with test buffer (5 mM Tris-HCl, 100 mM KCl, pH 7.0). Current measurement was taken out via a Keithley 2636A picoammeter (Keithley Instruments, Inc., Cleveland, OH). Transmembrane potential across the film was applied by placing two Ag/AgCl electrodes into each half of the cell (Scheme S1 in the Supporting Information). The scanning voltage used in this work was varied from −0.5 to +0.5 V. All the ion current signals were recorded and collected via ACS Basic 1.2 Software (Keithley Instruments, Inc., Cleveland, OH). The average current values at different voltages were obtained through three repeated tests.

Preparation and Functionalization of Nanochannels. The nanoporous PET films were fabricated through the ion track-etching technique. Generally, PET membrane was first exposed to the ultraviolet light (UV) for 1 h from each side. After that, the film was treated with hot NaOH solution (9 M, 50 °C) for several minutes (optimized from 6 to 10 min) and then quickly immersed into the stopping solution (1 M KCl + 1 M HCOOH) for 20 min at room temperature. Subsequently, the nanoporous membrane was carefully washed with deionized water and stored in deionized water overnight before use. To obtain streptavidin-modified membrane, the as-prepared nanoporous PET film was put into 0.1 M MES buffer (pH 6.0) containing 50 mM *N*-hydroxysuccinimide (NHS) and 100 mM *N*-ethyl-*N*-(3-dimethylaminopropyl)carbodiimide (EDC) for 30 min to activate the carboxyl groups on the channel walls. After rinsing with deionized water, the resulting PET membrane was then reacted with 0.2 mg/mL streptavidin in 0.1 M MES buffer (pH 6.0) overnight. The unbound area on the channel walls was blocked by incubating the film with 1 M glycine for 10 min in the dark. Finally, the functionalized PET membrane was gently washed with deionized water and then stored in the test buffer.

DNA Hybridization and Immobilization. The hybridization between P1-biotin (1 μM) and P2 (1.5 μM) was carried out in Tris-HCl buffer (20 mM Tris, 10 mM $MgCl_2$, pH 7.0) for 1 h (55 °C). The obtained biotin-dsDNA solution (about 1 μM) was stored at 4 °C for further use. Biotin-dsDNA was immobilized onto the channel walls through the strong affinity interactions between biotin and streptavidin. In order to evaluate the pore-blocking effect, streptavidin-modified nanoporous PET films were incubated with different amount of biotin-dsDNA in the reaction buffer (70 mM Tris-HCl, 10 mM $MgCl_2$, 5 mM DTT, pH 8.0) at room temperature. Current measurements were performed after rinsing the resulted films thoroughly with the test buffer. The concentration optimizations of streptavidin and biotin-dsDNA were 0.005−0.5 mg/mL, 0.01−1 μM, respectively. The incubation time for the affinity binding was optimized from 20 to 120 min.

dx.doi.org/10.1021/ac302875p | *Anal. Chem.* 2013, 85, 334−340

PNK-Catalyzed Phosphorylation and Assay Optimization. In a typical phosphorylation and cleavage experiment, 100 nM biotin-dsDNA, 0.5 mM ATP, 10 units of λ exo, and a certain amount of PNK were added into 100 μL of reaction buffer and incubated at 37 °C for 30 min. Then streptavidin-modified nanoporous PET film was immersed into the reaction mixture for 1 h, followed by test buffer washing and finally ion current measurement. The reaction pH was optimized from 7.0 to 9.0. The concentration optimizations of λ exo and ATP were 0.1−15 units and 0.01−5 mM, respectively.

Kinase Inhibitor Evaluation. In the inhibition assay, to investigate the effects of inhibitors on the PNK-catalyzed phosphorylation process, several kinds of inhibitors, including adenosine diphosphate (0.1−4 mM), $(NH_4)_2SO_4$ (1−25 mM), and Na_2HPO_4 (10−50 mM), were contained in the reaction buffer, respectively. After the addition of 100 nM dsDNA, 0.5 mM ATP, 10 units of λ exo, and 0.5 unit of PNK, the reaction was carried out at 37 °C for 30 min. The procedures were similar to the above.

Instruments. The scanning electron microscopy (SEM) image was recorded using a JSM-7401 field emission SEM system (JEOL, Japan). Attenuated total internal reflectance Fourier transform infrared spectroscopy (ATR-FT-IR) and Fourier transform-infrared spectroscopy (FT-IR) spectra were obtained via a Nicolet 6700 FT-IR spectrometer (Thermo Scientific). Fluorescence spectra were measured on a Multilabel plate Reader (PerkinElmer) at room temperature.

RESULTS AND DISCUSSION

Design of the Nanochannel Biosensor. Scheme 1 illustrates the developed strategy for PNK activity evaluation. Polyethylene terephthalate (PET, 12 μm thick, with ion track of $10^6/cm^2$) is a good candidate for preparing ion track pores with a high aspect ratio in a free-standing membrane. Ion beam irradiation and the chemical etching process produce plenty of carboxyl (−COOH) groups on the nanochannel walls. Taking advantage of the amide reaction between carboxyl and amino groups, streptavidin was successfully grafted on the surface of the nanochannels. Biotin-labeled dsDNA (biotin-dsDNA), which was obtained by the hybridization between biotin labeled oligonucleotide probe 1 (P1-biotin) and oligonucleotide probe 2 (P2), was further immobilized on the inner channel walls through the efficient streptavidin−biotin affinity interaction. Owing to the rigid duplex structure, biotin-dsDNA forms dense and stable macromolecular packing inside the nanochannel, resulting in an obvious pore-blocking effect[31] and sharp decrease of the ion current. When λ exocatalyzed biotin-dsDNA was incubated with the membrane, a similar phenomenon that ion current decreased greatly has also been found. It is ascribed to the fact that λ exo shows low catalytic efficiency toward dsDNA with the 5′-hydroxyl end. Therefore, biotin-dsDNA molecules are able to maintain their rigid double-strand structure and bring on distinct current blockage inside the channel. However, when the coupled exonuclease reaction was introduced, PNK first phosphorylated biotin-dsDNA at its 5′-hydroxyl end and then λ exo rapidly cleaved the 5′-phosphoryl termini product, yielding ssDNA (i.e., P2), mononucleotides, and biotin molecules. Although the affinity binding between biotin and streptavidin still exists, unfortunately, without the assistance given by dsDNA, small biotin molecules could no longer induce any obvious current decline. Thus the activity of PNK can be easily and sensitively reflected by the ion current signals change.

Scheme 1. Schematic Representation of the Nanochannel Biosensor for Polynucleotide Kinase Activity (PNK) Activity and Inhibition Detection[a]

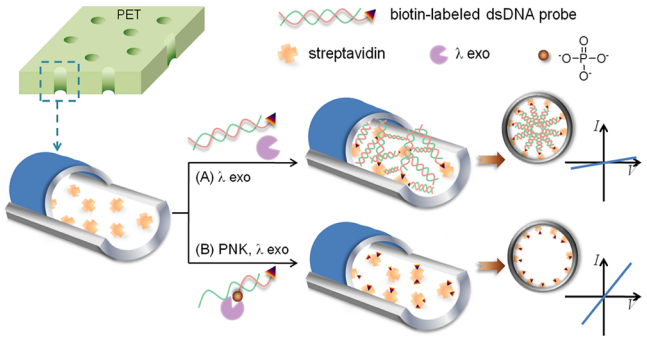

[a]The chemically etched nanoporous PET membrane was first modified with streptavidin through the amide reaction between carboxyl groups on the nanochannel wall and amino groups of the protein. (A) When biotin-dsDNA was incubated with the streptavidin-functionalized nanochannel, the formation of dense DNA arrangement inside the channel caused a significant pore-blocking effect and thus led to a much lower current response. (B) After biotin-dsDNA was phosphorylated by PNK and then immediately cleaved by λ exo, the remaining biotin small molecules could not induce an obvious current decline in spite of binding on the channel walls.

Functionalization of the Nanoporous PET Membranes. The nanochannels embedded in the $10^6/cm^2$ ion track-etched PET membrane were fabricated through the track-etching technique. This technique has been widely utilized in the manufacture of particular nanoporous polymer products. By using three steps of heavy ion irradiation, UV light exposure and chemical etching, pore density, size, as well as channel shapes can all be precisely controlled.[32] SEM image (Figure S1 in the Supporting Information) demonstrates that after etched by a hot concentrated sodium hydroxide (NaOH) solution for 8.5 min, the cylindrical nanochannels exhibit an average diameter of 60 ±10 nm. Carboxyl groups on the channel walls, which generated during the chemical etching, acted as the junctions for further immobilizing streptavidin. We recorded ATR-FT-IR spectra of the membrane to get insight on the surface modification.[33] It is observed from Figure S2 in the Supporting Information that streptavidin conjugated PET film shows two characteristic peaks at 1540 and 1650 cm^{-1}, corresponding to the amide II (N−H bending) and amide I (—C═O) bands of the protein, respectively. The peak at 3300 cm^{-1} was assigned the N−H/O−H stretching frequency of streptavidin.

Current measurement was applied to characterize the buildup process by monitoring the ion transport properties of the nanochannel. It has been reported that on the condition of using the same transmembrane voltage and electrolyte ion concentration, the ion current of PET nanopore is mainly dependent on two factors: the effective pore diameter and the charge distribution inside the nanopore.[34−37] As can been seen from Figure 1, bare nanochannel exhibits a linear current−voltage (I−V) curve without a rectification effect attributed to its cylindrical shape and symmetrical surface charge distribution (curve a).[38,39] When the film was grafted with streptavidin, the protein monolayer on the nanochannel wall led to a minor decrease of ion current (curve b). It is reasoned that covalently immobilized streptavidin partially blocks the inner nanochannel

dx.doi.org/10.1021/ac302875p | Anal. Chem. 2013, 85, 334−340

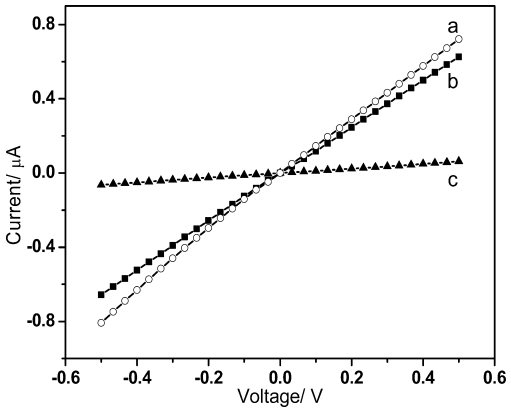

Figure 1. Current–voltage (I–V) characteristics of (a) bare nanochannels embedded in a chemically etched PET membrane, streptavidin-modified nanochannels (b) before and (c) after incubation with biotin-dsDNA in test buffer. The etching time, concentration of streptavidin and biotin-dsDNA, affinity incubation time were 8.5 min, 0.2 mg/mL, 0.1 μM, and 60 min, respectively.

and thus induces a reduction of the effective pore size.[40] The slight decrease of the ion current mainly originates from the relatively small dimensions of streptavidin (5.4 nm × 5.8 nm × 4.8 nm).[41] The current–voltage characteristics indicate the successful functionalization of streptavidin onto the inner walls of the nanochannels, which is consistent with the results obtained from the ATR-FT-IR method.

Pore-Blocking Effect Induced by Biotin-dsDNA. The covalent immobilization of streptavidin on the channel surface provides adequate binding sites for biotin-dsDNA. Moreover, the highly efficient affinity interaction between streptavidin and biotin ensure the binding efficiency of biotin-dsDNA. Figure 1 manifests that the ion current represents a sharp reduction after the streptavidin-modified nanochannels were incubated with biotin-dsDNA (curve c). The fact arises from the rigid duplex structures of dsDNA, which form closely packed arrangements inside the nanochannels and thus greatly decrease the effective pore diameter.[31] This phenomenon was also confirmed by fluorescence emission spectra as shown in Figure S3 in the Supporting Information. FAM labeled biotin-dsDNA (hybrid of P1-biotin and P3-FAM) was used as the report probe. Comparing with the streptavidin-modified PET film (curve a), the DNA attached PET membrane exhibits strong fluorescence emission around 520 nm with excitation at 497 nm (curve b), suggesting the effective assembly of biotin-dsDNA on the PET surface.

In our strategy, we used I_0/I to evaluate the dsDNA-induced pore-blocking effect, where I_0 and I are the current values of streptavidin-modified nanochannel and biotin-dsDNA attached nanochannel at −0.5 V, respectively. Higher I_0/I value not only means more effective pore-blocking effect but also provides more excellent analysis performance for the following PNK activity detection. Consequently, we optimized four main influencing factors to obtain a more desired I_0/I value, including the chemical etching time, concentration of streptavidin and biotin-dsDNA, as well as the affinity incubation time (Figure S4 in the Supporting Information). The optimal pore-etching time, concentrations of streptavidin and biotin-dsDNA, and affinity incubation time for the DNA binding procedure were 8.5 min, 0.2 mg/mL, 0.1 μM, and 60 min in these experiments, respectively.

PNK Monitoring Behavior of the Nanochannel Biosensor. Figure 2 demonstrates the I–V properties of the

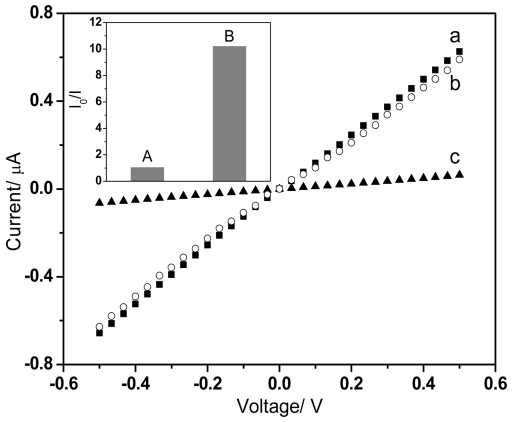

Figure 2. Current–voltage (I–V) characteristics and I_0/I values of (a) streptavidin-modified nanochannels, streptavidin-modified nanochannels assembled of biotin-dsDNA (b, inset $A = I_{0,a}/I_b$ at −0.5 V) with and (c, inset $B = I_{0,a}/I_c$ at −0.5 V) without PNK treatment in test buffer. The concentrations of biotin-dsDNA, ATP, λ exo, and PNK were 0.1 μM, 0.5 mM, 10 units, and 5 U mL^{-1}, respectively.

streptavidin-modified nanochannels after assembly of biotin-dsDNA with (curve b) and without (curve c) PNK treatment. Compared to the streptavidin-modified membranes (curve a), channels reacted with biotin-dsDNA catalyzed only by λ exo shows much lower current signal at the same voltage (curve c). On the contrary, the current signal decreased slightly when biotin-dsDNA catalyzed by both PNK and λ exo (curve b). It is observed from the inset of Figure 2 that the obtained I_0/I values under these two situations (inset $A = I_{0,a}/I_b$, inset $B = I_{0,a}/I_c$ at −0.5 V) exhibit nearly 10 times a difference. It is mainly ascribed to the fact that PNK catalyzes the transfer of the γ-phosphate group of ATP to the 5′-hydroxyl end of biotin-dsDNA, providing a preferred substrate (i.e., 5′-phosphorylated biotin-dsDNA) for λ exo. This exonuclease will promptly remove the 5′-phosphorylated mononucleotides from duplex DNA in a 5′ to 3′ direction. It is known that λ exo will also degrade nonphosphorylated substrate; however, the rate is over 300 times slower than that of dsDNA with a phosphate moiety at the 5′-dsDNA end.[42,43] Consequently, under the same experimental conditions, biotin-dsDNA catalyzed only by λ exo still maintain its original rigid duplex structure and thus result in a great reduction of the effective pore size, yielding a relative high I_0/I value. When biotin-dsDNA were phosphorylated by PNK and then rapidly hydrolyzed by λ exo, the remaining biotin-nucleotides could not cause any effective physical block inside the nanochannel. As a result, similar current signals of I and I_0 were found. The significant discrepancy of the I_0/I values indicates that combining with the coupled enzyme reaction system, the as-designed nanochannel platform can be used for kinase activity determination.

Optimization of Assay Conditions. In order to improve the kinase detection performance, we investigated effects of four main influencing factors on the sensor response. The reaction time is a crucial parameter for PNK-catalyzed phosphorylation and the coupled λ exo cleavage process. Although λ exo could only digest dsDNA from the 5′-hydroxyl end at a slow speed, nonetheless, it would also underlie unfavorable cleavage when a long incubation time was

dx.doi.org/10.1021/ac302875p | Anal. Chem. 2013, 85, 334–340

applied.[42] As shown in Figure 3A, with the increase of the reaction time, the I_0/I value of the nanochannel gradually

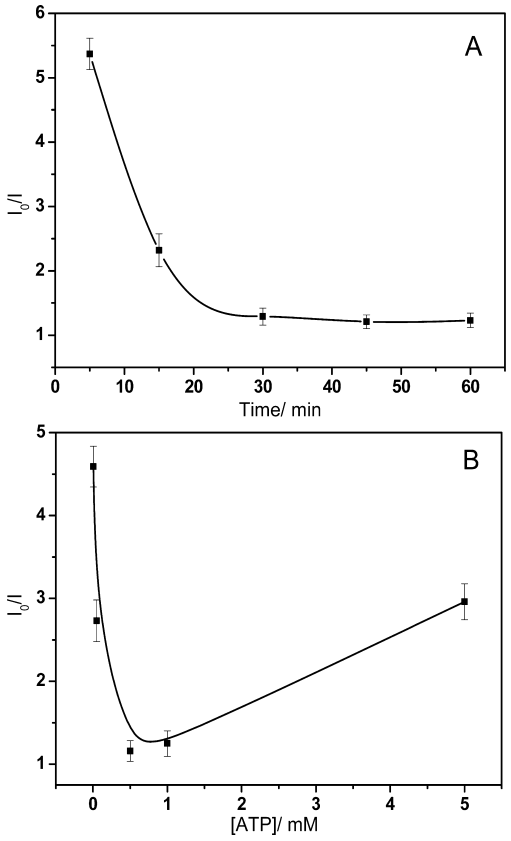

Figure 3. Optimization of (A) coupled-enzyme reaction time and (B) ATP concentration. The assays were all carried out in the reaction buffer, containing 0.1 μM biotin-dsDNA, 10 units λ exo, and 5 U mL^{-1} PNK (S/N = 3).

decreased and finally reached a plateau in 30 min, suggesting a tendency to complete the phosphorylation and cleavage process. Accordingly, the optimal reaction time was chosen to be 30 min.

ATP acts as the enzyme substrate and provides the phosphate group for 5′-hydroxyl dsDNA during the phosphorylation. It has been reported that either the absence or an excess of ATP will prohibit the kinase activity.[4] The amount of ATP has a strong influence on the efficiency of kinase-catalyzing reaction. Figure 3B demonstrates that the I_0/I values of the streptavidin-modified nanochannels reduced with the growing concentrations of ATP in the presence of PNK. The I_0/I value reached its minimum at the ATP concentration of 0.5 mM while started to increase when the ATP concentration further increased. The increasing I_0/I values imply the analytical performance degradation of the sensor at higher ATP concentration. This inhibition effect stems from the competitive binding between ATP and DNA to PNK, whose binding sites for DNA are partially blocked by ATP. Thus, the optimal concentration of ATP was 0.5 mM. Additionally, the other two important parameters, the amount of λ exo and pH of the reaction buffer were also optimized in our assay. As shown in Figure S5 in the Supporting Information, the amount of λ exo and the optimal pH for the coupled enzyme catalyzed procedure were 10 units and 8.0 in these experiments, respectively.

Current Measurement of PNK Activity. On the basis of the optimal experimental conditions, the as-proposed nanochannel biosensor was applied to investigate the activity of kinase at different concentrations of PNK. Measurements were performed three times for each test, and the results are presented in Figure 4. As can be seen, the I_0/I value decreased

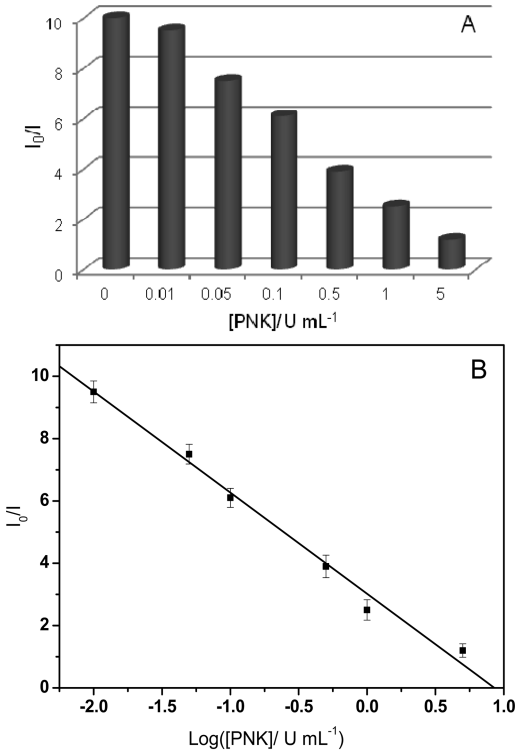

Figure 4. (A) I_0/I values with different activity units of PNK in reaction buffer. (B) The dependence of I_0/I value on the logarithm of PNK concentration. The concentrations of biotin-dsDNA, ATP, and λ exo were 0.1 μM, 0.5 mM, and 10 units, respectively.

along with the increasing PNK units varied from 0.01 to 5 U mL^{-1}. Figure 4B displays the dependence of the I_0/I value on the PNK concentration. The I_0/I value of the sensor exhibits a linear correlation to the logarithm of PNK concentration range from 0.01 to 5 U mL^{-1}. The linear relationship can be described as I_0/I = 2.988−3.790 log c with the correlation coefficient of R^2 = 0.994, where I_0 and I are the current values of the streptavidin-modified nanochannel before and after incubating with the coupled-enzyme treated biotin-dsDNA at −0.5 V, and log c is the logarithm of the PNK concentration. The detection limit of PNK was 0.01 U mL^{-1} (signal-to-noise ratio of 3), which was much lower than that of the previously reported ^{32}P-labeling methods and comparable to the results obtained from fluorescence assays.[4,12,17,44] The results indicate that sensitive and accurate kinase activity measurement can be achieved through the PNK-λ exo coupled enzyme catalytic system and the nanochannel-based sensing platform.

Evaluation of Kinase Activity Inhibition. The capacity of the nanochannel biosensor to detect the activity of PNK was also studied by evaluating the effectiveness of various kinase inhibitors, including adenosine diphosphate (ADP), ammonium sulfate, and sodium hydrogen phosphate. Because these chemicals are considered to have no inhibition effect on the activity of λ exo, all can be used as inhibitors for PNK. Half-

dx.doi.org/10.1021/ac302875p | Anal. Chem. 2013, 85, 334−340

maximal inhibition value IC_{50} was obtained by means of applying different concentrations of inhibitors in each inhibition assay. ADP is the product of the phosphorylation reaction. Continuous ADP accumulation in the reaction buffer will cause a severe inhibition effect on PNK activity due to the reversible property of the phosphorylation reaction.[4] Figure 5A presents the concentration dependent I_0/I value. As expected, merely 0.1 mM ADP had led to obvious increase of the I_0/I value. On the basis of the data, the IC_{50} of ADP was calculated to be 1 mM, which is consistent with the results obtained in the reported literature.[4,17] In addition, as shown in Figure 5B,C, the dose-dependence of inhibition by ammonium sulfate and sodium hydrogen phosphate were further measured. The 12 mM ammonium sulfate and 18.5 mM sodium hydrogen effectively suppressed the activity of PNK by around 50%, respectively. These results are also very close to the value determined elsewhere.[4,17] The salt effect on PNK activity may be attributed to two reasons. First, it is known that the activity of the enzyme mainly depends on its structure and conformation, which are significantly affected by several factors, such as ion strength, temperature, pH, and so on. Therefore, high concentration of salts probably induces the conformation change of the enzyme and further leads to the reduction of the kinase activity. Second, the reactivity of the 5′-hydroxyl group would possibly be inhibited because of the more stable dsDNA structure at high salt concentration.[45,46] These results manifest that the effect of various inhibitors on PNK can be quantitatively determined using the developed nanochannel biosensor.

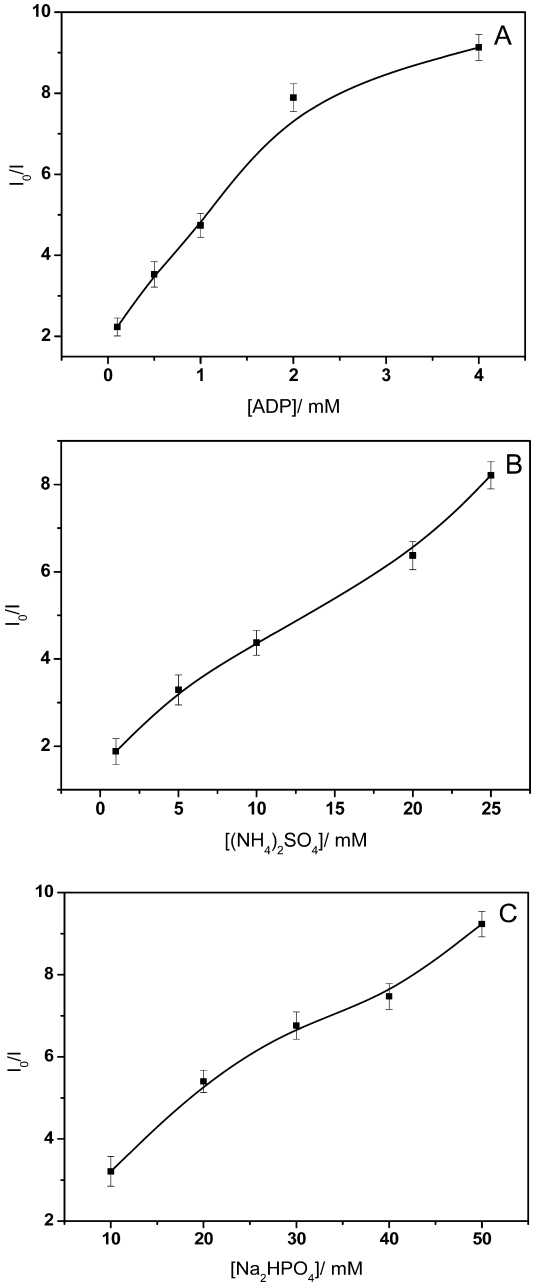

Figure 5. Inhibition effects of (A) ADP, (B) $(NH_4)_2SO_4$, and (C) Na_2HPO_4 on phosphorylation. The assays were carried out in the reaction buffer, containing 0.1 μM biotin-dsDNA, 5 U mL^{-1} PNK, 0.5 mM ATP, and 10 units λ exo.

CONCLUSION

In summary, a novel nanochannel biosensor based on a functionalized nanochannel system and coupled λ exo cleavage reaction has been developed for PNK activity and inhibition assay. Different amount of PNK changes the DNA package arrangements inside the channel and thus alters the effective pore size to a different extent. The kinase-induced microstructural distinctness can be conveniently and sensitively monitored through ion current signals using the nanochannel-based sensing system. Moreover, modification convenience and mechanical robustness ensure the stability of the test platform. The as-proposed nanochannel biosensor provides a highly sensitive approach for PNK activity screening with a low detection limit of 0.01 U mL^{-1} and a wide linear range from 0.01 to 5 U mL^{-1}. In addition, this strategy also exhibits excellent performance in evaluating the inhibition effects of ADP, ammonium sulfate, and sodium hydrogen phosphate on phosphorylation. We believe that the sensitive nanochannel biosensor has great potential for use in biological process research, drug discovery, and diagnostic applications.

ASSOCIATED CONTENT

Supporting Information

Additional information as noted in text. This material is available free of charge via the Internet at http://pubs.acs.org.

AUTHOR INFORMATION

Corresponding Author

*Phone: 86-10-62795290. Fax: 86-10-62771149. E-mail: jhli@mail.tsinghua.edu.cn.

Notes

The authors declare no competing financial interest.

ACKNOWLEDGMENTS

This work was financially supported by National Basic Research Program of China (Grant 2011CB935704), the National Natural Science Foundation of China (Grants 21235004 and 21128005), and the European Union Seventh Framework Programme (FP7/2007-2013) under Grant Agreement No. 260600 ("GlycoHIT").

REFERENCES

(1) Wang, L. K.; Lima, C. D.; Shuman, S. *EMBO J.* **2002**, *21*, 3873–3880.

(2) Whitehouse, C. J.; Taylor, R. M.; Thistlethwaite, A.; Zhang, H.; Karimi-Busheri, F.; Lasko, D. D.; Weinfeld, M.; Caldecott, K. W. *Cell* **2001**, *104*, 107−117.
(3) Ma, C. B.; Yeung, E. S. *Anal. Bioanal. Chem.* **2010**, *397*, 2279−2284.
(4) Tang, Z. W.; Wang, K. M.; Tan, W. H.; Ma, C. B.; Li, J.; Liu, L. F.; Guo, Q. P.; Meng, X. X. *Nucleic Acids Res.* **2005**, *33*, e97.
(5) Lown, J. W.; McLaughlin, L. W. *Biochem. Pharmacol.* **1979**, *28*, 1631−1638.
(6) Henner, W. D.; Rodriguez, L. O.; Hecht, S. M.; Haseltine, W. A. *J. Biol. Chem.* **1983**, *258*, 711−713.
(7) Torriglia, A.; Perani, P.; Brossas, J. Y.; Chaudun, E.; Treton, J.; Courtois, Y.; Counis, M. F. *Mol. Cell. Biol.* **1998**, *18*, 3612−3619.
(8) Richards, C. C. *Proc. Natl. Acad. Sci. U.S.A* **1965**, *54*, 158−165.
(9) Phillips, D. H.; Arlt, V. M. *Nat. Protoc.* **2007**, *2*, 2772−2781.
(10) Rasouli-Nia, A.; Karimi-Busheri, F.; Weinfeld, M. *Proc. Natl. Acad. Sci. U.S.A* **2004**, *101*, 6905−6910.
(11) Sharma, S.; Doherty, K. M.; Brosh, R. M. *Biochem. J.* **2006**, *398*, 319−337.
(12) Karimi-Busheri, F.; Daly, G.; Robins, P.; Canas, B.; Pappin, D. J. C.; Sgouros, J.; Miller, G. G.; Fakhrai, H.; Davis, E. M.; Le Beau, M. M.; Weinfeld, M. *J. Biol. Chem.* **1999**, *274*, 24187−24194.
(13) Amitsur, M.; Levitz, R.; Kaufmann, G. *EMBO J.* **1987**, *6*, 2499−2503.
(14) Meijer, M.; Karimi-Busher, F.; Huang, T. Y.; Weinfeld, M.; Young, D. *J. Biol. Chem.* **2002**, *277*, 4050−4055.
(15) Wilson, D. M.; Thompson, L. H. *Proc. Natl. Acad. Sci. U.S.A* **1997**, *94*, 12754−12757.
(16) Wang, L. K.; Shuman, S. *J. Biol. Chem.* **2001**, *276*, 26868−26874.
(17) Song, C.; Zhao, M. P. *Anal. Chem.* **2009**, *81*, 1383−1388.
(18) Wu, W. H.; Hu, H. Y.; Li, F.; Wang, L. H.; Gao, J. M.; Lu, J. X.; Fan, C. H. *Chem. Commun.* **2011**, *47*, 1201−1203.
(19) Dekker, C. *Nat. Nanotechnol.* **2007**, *2*, 209−215.
(20) Siwy, Z. S.; Howorka, S. *Chem. Soc. Rev.* **2010**, *39*, 1115−1132.
(21) Hou, X.; Jiang, L. *ACS Nano* **2009**, *3*, 3339−3342.
(22) Vlassiouk, I.; Kozel, T. R.; Siwy, Z. S. *J. Am. Chem. Soc.* **2009**, *131*, 8211−8220.
(23) Ervin, E. N.; White, R. J.; White, H. S. *Anal. Chem.* **2009**, *81*, 533−537.
(24) Lathrop, D. K.; Ervin, E. N.; Barrall, G. A.; Keehan, M. G.; Kawano, R.; Krupka, M. A.; White, H. S.; Hibbs, A. H. *J. Am. Chem. Soc.* **2010**, *132*, 1878−1885.
(25) Ali, M.; Yameen, B.; Neumann, R.; Ensinger, W.; Knoll, W.; Azzaroni, O. *J. Am. Chem. Soc.* **2008**, *130*, 16351−16357.
(26) Iqbal, S. M.; Akin, D.; Bashir, R. *Nat. Nanotechnol.* **2007**, *2*, 243−248.
(27) Sa, N.; Fu, Y.; Baker, L. A. *Anal. Chem.* **2010**, *82*, 9963−9966.
(28) Vilozny, B.; Actis, P.; Seger, R. A.; Vallmajo-Martin, Q.; Pourmand, N. *Anal. Chem.* **2011**, *83*, 6121−6126.
(29) Ali, M.; Tahir, M. N.; Siwy, Z.; Neumann, R.; Tremel, W.; Ensinger, W. *Anal. Chem.* **2011**, *83*, 1673−1680.
(30) Han, C.; Hou, X.; Zhang, H.; Guo, W.; Li, H.; Jiang, L. *J. Am. Chem. Soc.* **2011**, *133*, 7644−7647.
(31) Hou, X.; Guo, W.; Xia, F.; Nie, F. Q.; Dong, H.; Tian, Y.; Wen, L.; Wang, L.; Cao, L.; Yang, Y.; Xue, J.; Song, Y.; Wang, Y.; Liu, D.; Jiang, L. *J. Am. Chem. Soc.* **2009**, *131*, 7800−7805.
(32) Apel, P. *Radiat. Meas.* **2001**, *34*, 559−566.
(33) Radhakumary, C.; Sreenivasan, K. *Anal. Chem.* **2011**, *83*, 2829−2833.
(34) Xia, F.; Guo, W.; Mao, Y.; Hou, X.; Xue, J.; Xia, H.; Wang, L.; Song, Y.; Ji, H.; Ouyang, Q.; Wang, Y.; Jiang, L. *J. Am. Chem. Soc.* **2008**, *130*, 8345−8350.
(35) Harrell, C. C.; Siwy, Z. S.; Martin, C. R. *Small* **2006**, *2*, 194−198.
(36) Siwy, Z. S. *Adv. Funct. Mater.* **2006**, *16*, 735−746.
(37) Powell, M. R.; Sullivan, M.; Vlassiouk, I.; Constantin, D.; Sudre, O.; Martens, C. C.; Eisenberg, R. S.; Siwy, Z. S. *Nat. Nanotechnol.* **2008**, *3*, 51−57.
(38) Ali, M.; Yameen, B.; Cervera, J.; Ramírez, P.; Neumann, R.; Ensinger, W.; Knoll, W.; Azzaroni, O. *J. Am. Chem. Soc.* **2010**, *132*, 8338−8348.
(39) Ali, M.; Ramirez, P.; Mafé, S.; Neumann, R.; Ensinger, W. *ACS Nano* **2009**, *3*, 603−608.
(40) Nilsson, J.; Lee, J. R. I.; Ratto, T. V.; Letant, S. E. *Adv. Mater.* **2006**, *18*, 427−431.
(41) Wilson, J. T.; Cui, W.; Chaikof, E. L. *Nano Lett.* **2008**, *8*, 1940−1948.
(42) Little, J. W. *J. Biol. Chem.* **1967**, *242*, 679−686.
(43) Perkins, T. T.; Dalal, R. V.; Mitsis, P. G.; Block, S. M. *Science* **2003**, *301*, 1914−1918.
(44) Lin, L.; Liu, Y.; Zhao, X.; Li, J. H. *Anal. Chem.* **2011**, *83*, 8396−8402.
(45) Lillehaug, J. R.; Kleppe, K. *Biochemistry* **1975**, *14*, 1225−1229.
(46) Lillehaug, J. R.; Kleppe, R. K.; Kleppe, K. *Biochemistry* **1976**, *15*, 1858−1865.